PROCEEDINGS OF SCIENCE

Decomposition of the proton spin from lattice QCD

K. Hadjiyiannakou,[a,b,*] **C. Alexandrou,**[a,b] **S. Bacchio,**[b] **M. Constantinou,**[c] **J. Finkenrath,**[b] **K. Jansen,**[d] **G. Koutsou,**[b] **H. Panagopoulos**[a] **and G. Spanoudes**[b]

[a] *Department of Physics, University of Cyprus, P.O. Box 20537, 1678 Nicosia, Cyprus*

[b] *Computation-based Science and Technology Research Center, The Cyprus Institute, Kavafi Street, Nicosia 2121, Cyprus*

[c] *Department of Physics, Temple University, 1925 N. 12th Street,Philadelphia, Pennsylvania 19122-1801, USA*

[d] *NIC, DESY, Platanenallee 6, D-15738 Zeuthen, Germany*

E-mail: k.hadjiyiannakou@cyi.ac.cy

The gluon and quark contributions to the proton spin are computed using an ensemble of gauge configurations with twisted mass Wilson fermions with masses tuned to approximately reproduce their physical values. A non-perturbative renormalization is carried out for both quark and gluon matrix elements. The contribution of up, down, strange and charm quarks to the proton intrinsic spin, orbital angular momentum and angular momentum are determined. All scale and scheme dependent quantities are given in the $\overline{\text{MS}}$ scheme at 2 GeV.

The 38th International Symposium on Lattice Field Theory, LATTICE2021 26th-30th July, 2021 Zoom/Gather@Massachusetts Institute of Technology

*Speaker

© Copyright owned by the author(s) under the terms of the Creative Commons Attribution-NonCommercial-NoDerivatives 4.0 International License (CC BY-NC-ND 4.0).

PoS(LATTICE2021)348

1. Introduction

The proton is composed of quarks and gluons, therefore its spin arises from the intrinsic spin and orbital angular momentum of its constituents. The E80 [1, 2] and E130 [3, 4] experiments at SLAC carried out the first study of the proton spin. A surprise result emerged from the studies of the European Muon Collaboration (EMC) [5, 6], namely it was found that less than a quarter of the proton spin comes from its valence quarks triggering the so-called proton spin puzzle. Recent experiments using polarized deep inelastic lepton-nucleon scattering (DIS) processes indeed confirmed that only about 25-30% [7–12] of the nucleon spin comes from the valence quark spin. For the strange quark, phenomenological analyses point to a negative value but their error is large [7, 11, 13–15]. Additionally, the gluon helicity carries large uncertainties as determined using inclusive DIS experiments. The Relativistic Heavy Ion Collider (RHIC) [16–18] at BNL up to now provides only constraints on $\int_{0.05}^{0.2} \Delta g(x)dx = 0.005^{+0.129}_{-0.164}$.

In this study we provide the *complete decomposition* of the proton spin. We compute both valence and sea quark contributions, as well as the gluon contribution to the spin and momentum fraction of the proton. For the evaluation of the quark loop contributions that are computationally demanding, we use improved techniques developed in recent years [19], as well as noise reduction methods [20, 21]. Compared to our previous work [22], several improvements are achieved: i) Ref. [22] used an ensemble of two degenerate light quarks ($N_f = 2$) [23], while in this work we use an ensemble of twisted mass fermions [24, 25] that includes, light, strange and the charm quarks all with masses fixed to their physical values ($N_f = 2 + 1 + 1$); ii) a more elaborated analysis of excited state contributions is carried out; iii) larger statistics are used; iv) calculation of the gluon contribution to the proton spin includes the generalized form factor $B_{20}(0)$; and v) non-perturbative renormalization is carried out for both the quark and the gluon operators.

The starting point is the traceless Energy-Momentum Tensor (EMT), which can be composed into a quark

$$\bar{T}_q^{\mu\nu} = \bar{\psi} i\gamma^{\{\mu} \overleftrightarrow{D}^{\nu\}} \psi \tag{1}$$

and a gluon component

$$\bar{T}_g^{\mu\nu} = F^{\{\mu\rho} F^{\nu\}}{}_{\rho}. \tag{2}$$

$F^{\mu\nu}$ is the gluon field-strength tensor and the notation $\{\cdots\}$ means symmetrization over μ, ν and subtraction of the trace and $\overleftrightarrow{D} = (\overleftarrow{D} + \overrightarrow{D})/2$ is the symmetrized covariant derivative. As discussed in Refs. [26, 27], the gauge invariant angular momentum operator is given by

$$\vec{J}_g = \int d^3x \, (\vec{x} \times (\vec{E} \times \vec{B})), \tag{3}$$

where $\vec{E}$ and $\vec{B}$ are the chromo-electric and chromo-magnetic fields. The quark angular momentum operator is given by

$$\vec{J}_q = \int d^3x \left[\bar{\psi} \frac{\vec{\gamma}\gamma^5}{2} \psi + \bar{\psi} (\vec{x} \times i\overrightarrow{D}) \psi \right], \tag{4}$$

where the first term is identified as the intrinsic quark spin operator $\Delta\Sigma_q$ and the second term is the quark orbital angular momentum L_q.

PoS(LATTICE2021)348

The nucleon matrix elements of the EMT entering in the evaluation of the contribution to the proton spin decomposes in three generalized form factors (GFFs) $A_{20}(q^2)$, $B_{20}(q^2)$ and $C_{20}(q^2)$ as follows [27] in Minkowski space,

$$\langle N(p',s')|T^{\mu\nu}_{q,g}|N(p,s)\rangle = \bar{u}_N(p',s')\Bigg[A^{q,g}_{20}(q^2)\gamma^{\{\mu}P^{\nu\}} + B^{q,g}_{20}(q^2)\frac{i\sigma^{\{\mu\rho}q_\rho P^{\nu\}}}{2m_N} + C^{q,g}_{20}(q^2)\frac{q^{\{\mu}q^{\nu\}}}{m_N}\Bigg]u_N(p,s), \tag{5}$$

where $u_N(p,s)$ is the nucleon spinor with momentum p and spin s, $P = (p'+p)/2$ is the average momentum and $q = p' - p$ the momentum transfer. In the forward limit the $A^{q,g}_{20}(0)$ gives the quark and gluon average momentum fraction $\langle x\rangle^{q,g}$ where $\sum_q \langle x\rangle^q + \langle x\rangle^g = 1$. As discussed in Ref. [26], the nucleon spin can be written in terms of A_{20} and B_{20} in the forward limit

$$J_N = \frac{1}{2}\left[A^{q+g}_{20}(0) + B^{q+g}_{20}(0)\right] = \frac{1}{2}, \tag{6}$$

which together with the momentum sum relations leads to that $\sum_q B^{q+g}_{20}(0) = 0$. Although the average momentum fractions are directly accessible at zero momentum transfer as can be seen from Eq. (5), the $B_{20}(0)$ are extracted after extrapolation from finite momentum transfers. Since we have a direct way to compute J^q_N and $\frac{\Delta\Sigma^q_N}{2}$, we can implicitly determine the quark orbital angular momentum via

$$L^q_N = J^q_N - \frac{\Delta\Sigma^q_N}{2}. \tag{7}$$

2. Ensemble and Statistics

In Table 1 we give the parameters of the $N_f = 2+1+1$ ensemble analyzed in this work denoted as cB211.072.64 [28]. The ensemble is produced using the Iwasaki [29] improved gauge action and the twisted mass fermion formulation [24, 25]. A clover term [30] is added to stabilize the simulations. The twisted mass fermion formulation is very well suited for hadron structure providing an automatic $O(a)$ improvement [25] with no need of improving the operators.

Table 1: Simulation parameters for the cB211.072.64 [28] ensemble, c_{SW} is the value of the clover coefficient, $\beta = 6/g$ where g is the coupling constant, N_f is the number of dynamical quark flavors in the simulation, a is the lattice spacing, V the lattice volume in lattice units, m_π the pion mass, m_N the nucleon mass, and L the spatial lattice extent in physical units.

$c_{\rm SW}$	β	N_f	a [fm]	V	$m_\pi L$	m_N/m_π	m_π [GeV]	L [fm]
1.69	1.778	2+1+1	0.0801(4)	$64^3 \times 128$	3.62	6.74(3)	0.1393(7)	5.12(3)

We analyze in total 750 configurations separated by 4 trajectories. For the computation of the connected three-point functions we use seven values of the sink-source time separation t_s ranging from 0.64 fm to 1.60 fm. In order to keep the signal-to-noise ratio approximately constant we increase the number of source positions as we increase t_s. The statistics used for each value of t_s

PoS(LATTICE2021)348

are given in Table 2. For the computation of the disconnected quarks loops we use a combination of noise reduction algorithms, such as the one-end trick, deflation of the low modes, spin color dilution and hierarchical probing. Details on these algorithms can be found in Ref. [31]. The statistics are given in Table 2.

Table 2: Left: Parameters used for the evaluation of the connected three-point functions. In the first column we give the value of t_s in lattice units and in the second column in physical units. In all cases 750 gauge configurations are analyzed. In the third column we give the number of source positions, and in the fourth column the total number of measurements. The last column gives N_{inv}, which is the total number of inversions per configuration. Right: Parameters and statistics used for the evaluation of the disconnected three-point functions. The number of source positions used for the evaluation of the two-point functions is $N_{\text{srcs}} = 200$ per gauge configuration. In the case of the light quarks, we compute the lowest 200 modes exactly and deflate before computing the higher modes stochastically. N_r is the number of noise vectors, and N_{Had} the number of Hadamard vectors. $N_{\text{sc}} = 12$ corresponds to spin-color dilution and N_{inv} is the total number of inversions per configuration.

t_s/a	t_s [fm]	N_{srcs}	N_{meas}	N_{inv}
8	0.64	1	750	120
10	0.80	2	1500	240
12	0.96	4	3000	480
14	1.12	6	4500	720
16	1.28	16	12000	1920
18	1.44	48	36000	5760
20	1.60	64	48000	7680

Flavor	N_{def}	N_r	N_{Had}	N_{sc}	N_{inv}
light	200	1	512	12	6144
strange	0	1	512	12	6144
charm	0	12	32	12	4608

3. Results

In order to extract the ground state matrix elements we compose a ratio of three- to two-point correlation functions and implement three methods to ensure that excited states contamination is sufficiently suppressed. Namely, we use the plateau method that assumes the lowest state dominates, the summation method where one sums the ratio over the insertion time taking into account the lowest state and a two-state fit approach that takes into account in addition to the lowest the first excited state. Fig. 1 shows the connected contribution to $\langle x \rangle_B^{u^+ + d^+}$. As can be seen, from the results of the ratio, the value decreases as the source-sink separation increases indicating a severe excited state contamination. This is corroborated by the middle panel showing the predicted trend using the parameters extracted from the two-state fit. The two-state fit method shows clear convergence as a function of the lowest point included in the fit and is compatible with the result extracted from the summation method at larger time separations. Therefore, we use as final value, the one determined from the two-state fit. The corresponding results for disconnected contributions can be found in Ref. [31].

In order to renormalize properly the EMT, since its quark components mix with the gluon, one needs a 2×2 mixing matrix, which has in the diagonal the multiplicative renormalization functions (Z_{qq}, Z_{gg}) and in the off-diagonal the mixing coefficients (Z_{qg}, Z_{gq}). For the computation of

PoS(LATTICE2021)348

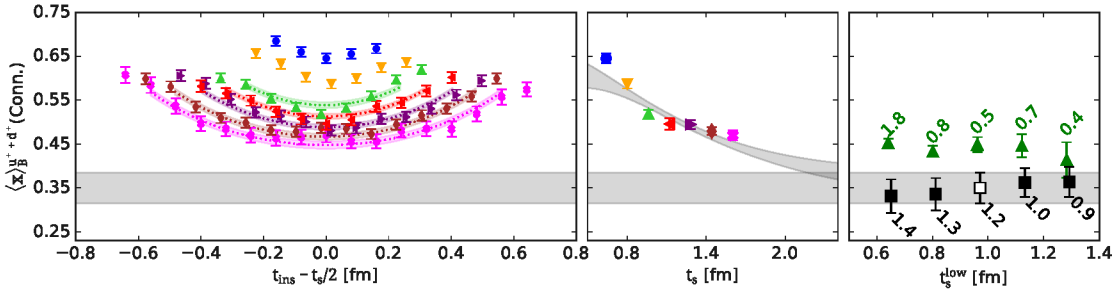

Figure 1: Excited state analysis for determining the connected isoscalar average momentum fraction $\langle x\rangle_B^{u^+d^+}$. In the left panel, we show results for the ratio for source-sink separations $t_s/a = 8, 10, 12, 14, 16, 18, 20$ using blue circles, orange down triangles, up green triangles, left red triangles, right purple triangles, brown rhombus, magenta crosses, respectively. The results are shown as a function of the insertion time $t_{\rm ins}$ shifted by $t_s/2$. The dotted lines and associated error bands are the resulting two-state fits. In the middle panel, we show the plateau values or middle point when no plateau is identified, as a function of source-sink separation using the same symbol used for the ratio in the left panel for the same t_s. The grey band is the predicted time-dependence of the ratio using the parameters extracted from the two-state fit when $t_s^{\rm low} = 12a = 0.96$ fm. In the right panel, we show values extracted using the two-state fit (black squares) and the summation method (green filled triangles) as a function of $t_s^{\rm low}$ together with the χ^2/d.o.f for each fit. The open symbol shows the selected value for the connected $\langle x\rangle_B^{u^+d^+}$ with the grey band spanning the whole range of the figure being its statistical error.

the Green's functions we use the Rome-Southampton scheme and employ the momentum source method to increase statistical precision. An important aspect of our renormalization program is the improvement of the non-perturbative estimates by subtracting finite-a effects [32, 33], calculated to one-loop in lattice perturbation theory and to all orders in the lattice spacing, $O(g^2\, a^\infty)$. In Fig. 2, we present the case of Z_{qq} for both singlet and non-singlet flavor combinations. As can be seen, subtracting the lattice artifacts is an important factor in reducing finite a effects. It is worth mentioning that the singlet combination due to the inclusion of disconnected contributions has bigger errors. The computation of the Z_{gg} is also performed non-perturbatively. More details on this determination can be found in Ref. [31]. The computation of the mixing components are done in perturbation theory up to one loop order.

The renormalized results then are obtained from the expressions

$$X_R^{q^+} = Z_{qq} X_B^{q^+} + \frac{\delta Z_{qq}}{N_f} \sum_{q=u,d,s,c} X_B^{q^+} + \frac{Z_{qg}}{N_f} X_B^g \tag{8}$$

and

$$X_R^g = Z_{gg} X_B^g + Z_{gq} \sum_{q=u,d,s,c} X_B^{q^+}, \tag{9}$$

where $X = \langle x\rangle, J$ and δZ_{qq} is the difference between singlet and non-singlet Z_{qq} and $N_f = 4$ since we use a massless renormalization scheme and thus need to take the chiral limit.

PoS(LATTICE2021)348

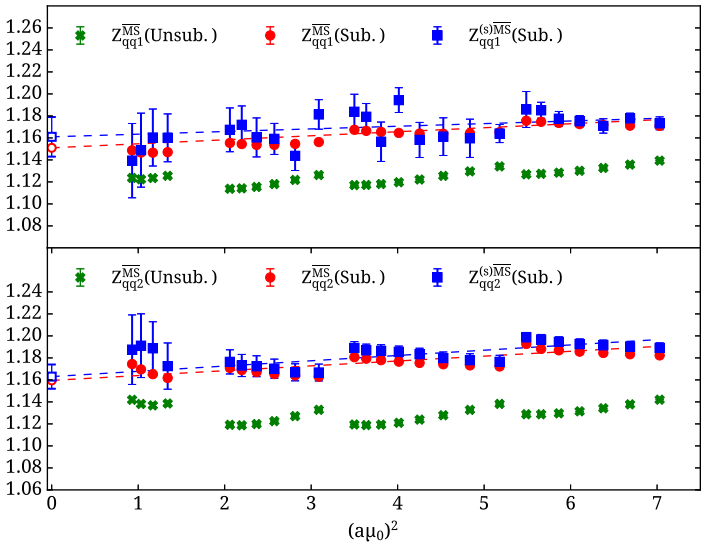

Figure 2: $\overline{Z}^{\overline{\rm MS}}_{qq1}$ (upper) and $\overline{Z}^{\overline{\rm MS}}_{qq2}$ (bottom) as a function of the initial RI′ scale $(a\,\mu_0)^2$. The purely non-perturbative data are shown with green crosses, and the improved estimates after the subtraction of $O(g^2a^\infty)$-terms are shown with red circles. The blue squares show results of the singlet case after substraction of lattice artifacts. The dashed lines show linear fits, and the extrapolated values with an open symbol.

Fig. 3 shows our results for the proton average momentum fraction for both quarks and gluons. The up quark gives the largest quark contribution, twice bigger than the down quark. The strange quark is significantly smaller, about 5% of the total spin and the charm is only 2%. The gluon a larger contribution of about 45% of the total proton spin. Summing all the contributions confirms the expected momentum sum. Fig. 3 also highlights that disconnected are very important and if excluded would result to a significant underestimation of the momentum sum. The individual contributions to the proton spin from the angular momentum are presented in Fig. 4 as extracted from Eq. (6). The major contribution comes from the up quark amounting to about 40% of the proton spin. The down, strange and charm quarks have relatively smaller contributions. All quark flavors together constitute to about 60% of the proton spin. The gluon contribution is significant, namely about 40% of the proton spin, providing the missing piece to satisfy the spin sum, namely 94.6(14.2)(2.8)%.

In Fig. 4 we show our results for $\frac{1}{2}\Delta\Sigma^{q^+} = \frac{1}{2}g_A^{q^+}$, where g_A is the axial charge. The up quark has a positive large contribution, the down quark contributes about half compared to the up and with opposite sign. Strange and charm quarks also have a negative contribution with the latter being about five times smaller than the former giving a 1% contribution.

Having both the quark angular momentum and the quark intrinsic spin allows us to extract the orbital angular momentum using Eq. (7). Our results are shown in Fig. 4. The orbital angular momentum of the up quark is negative reducing the total angular momentum contribution of the up quark to the proton spin. The contribution of the down quark to the orbital angular momentum is positive almost canceling the negative intrinsic spin contribution resulting to a relatively small positive contribution to the spin of the proton.

PoS(LATTICE2021)348

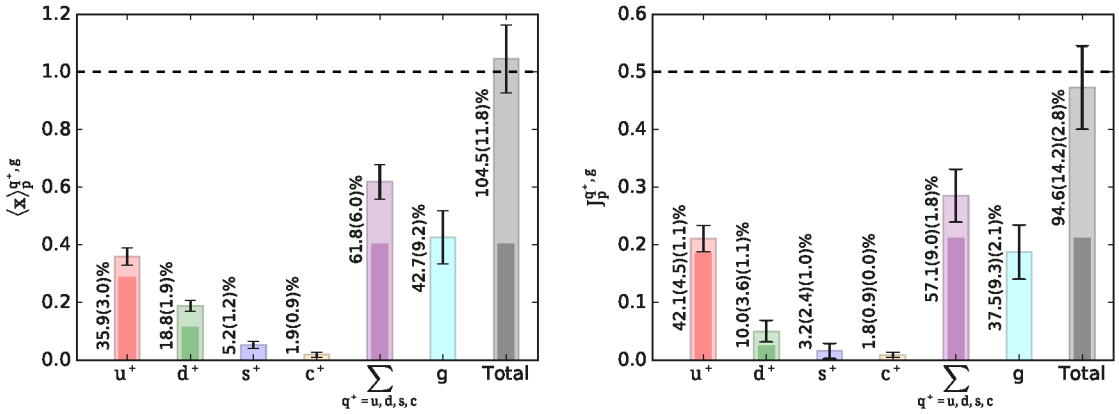

Figure 3: Left: The decomposition of the proton average momentum fraction $\langle x \rangle$. We show the contribution of the up (red bar), down (green bar), strange (blue bar), charm (orange bar), quarks and their sum (purple bar), the gluon (cyan bar) and the total sum (grey bar). Whenever two overlapping bars appear the inner bar denotes the purely connected contribution while the outer one is the total contribution which includes disconnected taking into account also the mixing. The error bars for the former are omitted while for the latter are shown explicitly on the bars. The percentages written in the figure are for the total contribution. Right: The total angular momentum J. The notation is as the left.

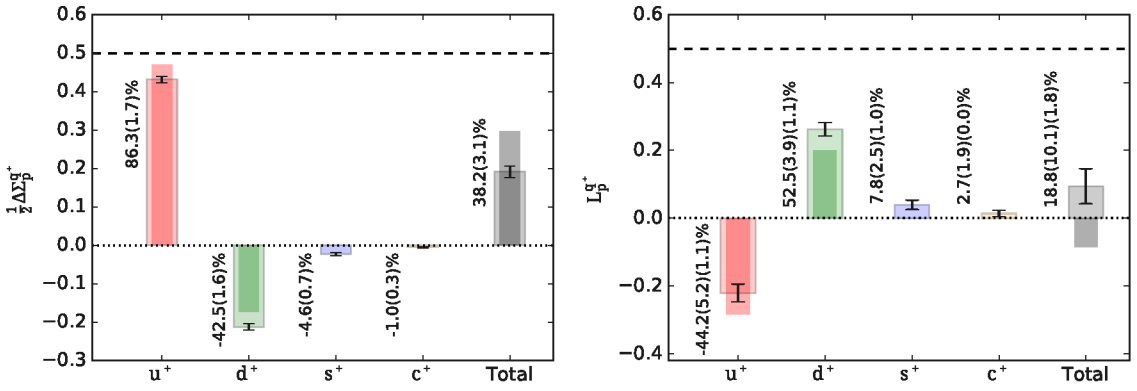

Figure 4: Left: Results for the intrinsic quark spin $\frac{1}{2}\Delta\Sigma_p^{q+}$ and right the quark orbital angular momentum L_p^{q+}.

4. Conclusions

The various contributions to the proton spin [31] are presented. The major outcomes are:

i) The contribution of quarks to the intrinsic proton spin is found to be: $\frac{1}{2}\sum_{q=u,d,s,c}\Delta\Sigma^{q^+} = 0.191(15)$. This is in agreement with the upper bound of the COMPASS value $0.13 \leq \frac{1}{2}\Delta\Sigma \leq 0.18$ [34]. It is worth mentioning that our value for $\frac{1}{2}\Delta\Sigma^{c^+} = -0.005(2)$ is the most precise determination to date.

ii) The verification of the momentum sum for the proton computing all the contributions: $\langle x\rangle^{u^+}+\langle x\rangle^{d^+}+\langle x\rangle^{s^+}+\langle x\rangle^{c^+}+\langle x\rangle^{g} = 0.359(30)+0.188(19)+0.052(12)+0.019(9)+0.427(92) = 1.045(118)$.

PoS(LATTICE2021)348

iii) The verification of spin sum of the proton. We find for the quark angular momentum $J^{u^+} + J^{d^+} + J^{s^+} + J^{c^+} + J^g = 0.211(22)(5) + 0.050(18)(5) + 0.016(12)(5) + 0.009(5)(0) + 0.187(46)(10) = 0.473(71)(14)$.

iv) The computation of the quark orbital angular momentum given by $\sum_{q=u,d,s,c} L^{q^+} = 0.094(51)(9)$.

In the near future we plan to compute these quantities on two ensembles with smaller lattice spacings in order to perform the continuum limit directly at the physical point.

Acknowledgments

K.H. is financially supported by the Cyprus Research Promotion foundation under contract number POST-DOC/0718/0100 and EuroCC project funded by the Deputy Ministry of Research, Innovation and Digital Policy and the Cyprus Research and Innovation Foundation and the European High-Performance Computing Joint Undertaking (JU) under grant agreement No 951732. The JU receives support from the European Union's Horizon 2020 research and innovation programme. The authors gratefully acknowledge the Gauss Centre for Supercomputing e.V. (www.gauss-centre.eu) for funding the project pr74yo by providing computing time on the GCS Supercomputer SuperMUC at Leibniz Supercomputing Centre (www.lrz.de). Results were obtained using Piz Daint at Centro Svizzero di Calcolo Scientifico (CSCS), via the project with id s702. We thank the staff of CSCS for access to the computational resources and for their constant support.

References

[1] M. J. Alguard et al., Phys. Rev. Lett. **37**, 1261 (1976), [,289(1976)].

[2] M. J. Alguard et al., Phys. Rev. Lett. **41**, 70 (1978), [,294(1978)].

[3] G. Baum et al., Phys. Rev. Lett. **45**, 2000 (1980), [,298(1980)].

[4] G. Baum et al., Phys. Rev. Lett. **51**, 1135 (1983), [,302(1983)].

[5] J. Ashman et al. (European Muon), Phys. Lett. **B206**, 364 (1988), [,340(1987)].

[6] J. Ashman et al. (European Muon), Nucl. Phys. **B328**, 1 (1989), [,351(1989)].

[7] D. de Florian, R. Sassot, M. Stratmann, and W. Vogelsang, Phys. Rev. Lett. **101**, 072001 (2008), 0804.0422.

[8] D. de Florian, R. Sassot, M. Stratmann, and W. Vogelsang, Phys. Rev. **D80**, 034030 (2009), 0904.3821.

[9] J. Blumlein and H. Bottcher, Nucl. Phys. **B841**, 205 (2010), 1005.3113.

[10] E. Leader, A. V. Sidorov, and D. B. Stamenov, Phys. Rev. **D82**, 114018 (2010), 1010.0574.

[11] R. D. Ball, S. Forte, A. Guffanti, E. R. Nocera, G. Ridolfi, and J. Rojo (NNPDF), Nucl. Phys. **B874**, 36 (2013), 1303.7236.

PoS(LATTICE2021)348

[12] A. Deur, S. J. Brodsky, and G. F. De Téramond, Rept. Prog. Phys. **82** (2019), 1807.05250.

[13] H.-W. Lin et al., Prog. Part. Nucl. Phys. **100**, 107 (2018), 1711.07916.

[14] E. R. Nocera, R. D. Ball, S. Forte, G. Ridolfi, and J. Rojo (NNPDF), Nucl. Phys. **B887**, 276 (2014), 1406.5539.

[15] X. Liu and B.-Q. Ma, Eur. Phys. J. **C79**, 409 (2019), 1905.02360.

[16] E. C. Aschenauer et al. (2013), 1304.0079.

[17] P. Djawotho (STAR), Nuovo Cim. **C036**, 35 (2013), 1303.0543.

[18] A. Adare et al. (PHENIX), Phys. Rev. **D90**, 012007 (2014), 1402.6296.

[19] C. Alexandrou, M. Constantinou, V. Drach, K. Hadjiyiannakou, K. Jansen, G. Koutsou, A. Strelchenko, and A. Vaquero, Comput. Phys. Commun. **185**, 1370 (2014), 1309.2256.

[20] A. Stathopoulos, J. Laeuchli, and K. Orginos (2013), 1302.4018.

[21] C. Michael and C. Urbach (ETM), PoS **LATTICE2007**, 122 (2007), 0709.4564.

[22] C. Alexandrou, M. Constantinou, K. Hadjiyiannakou, K. Jansen, C. Kallidonis, G. Koutsou, A. Vaquero Avilés-Casco, and C. Wiese, Phys. Rev. Lett. **119**, 142002 (2017), 1706.02973.

[23] A. Abdel-Rehim et al. (ETM), Phys. Rev. **D95**, 094515 (2017), 1507.05068.

[24] R. Frezzotti, P. A. Grassi, S. Sint, and P. Weisz (Alpha), JHEP **08**, 058 (2001), hep-lat/0101001.

[25] R. Frezzotti and G. C. Rossi, JHEP **08**, 007 (2004), hep-lat/0306014.

[26] X.-D. Ji, Phys. Rev. Lett. **78**, 610 (1997), hep-ph/9603249.

[27] X.-D. Ji, J. Phys. **G24**, 1181 (1998), hep-ph/9807358.

[28] C. Alexandrou et al., Phys. Rev. **D98**, 054518 (2018), 1807.00495.

[29] Y. Iwasaki, Nucl. Phys. **B258**, 141 (1985).

[30] B. Sheikholeslami and R. Wohlert, Nucl. Phys. **B259**, 572 (1985).

[31] C. Alexandrou, S. Bacchio, M. Constantinou, J. Finkenrath, K. Hadjiyiannakou, K. Jansen, G. Koutsou, H. Panagopoulos, and G. Spanoudes, Phys. Rev. D **101**, 094513 (2020), 2003.08486.

[32] M. Constantinou, R. Horsley, H. Panagopoulos, H. Perlt, P. E. L. Rakow, G. Schierholz, A. Schiller, and J. M. Zanotti, Phys. Rev. **D91**, 014502 (2015), 1408.6047.

[33] C. Alexandrou, M. Constantinou, and H. Panagopoulos (ETM), Phys. Rev. **D95**, 034505 (2017), 1509.00213.

[34] C. Adolph et al. (COMPASS), Phys. Lett. **B753**, 18 (2016), 1503.08935.

PoS(LATTICE2021)348